Fabrication and characterisation of high-performance joints made of ZrB_2-SiC ultra-high temperature ceramics

Xiaochao Jin, Jingjing Yang, Yongle Sun, Pan Li, Cheng Hou, Yuxiang Zhao, Xueling Fan

PII: S0955-2219(21)00585-9

DOI: https://doi.org/10.1016/j.jeurceramsoc.2021.08.018

Reference: JECS 14261

To appear in: *Journal of the European Ceramic Society*

Received Date: 8 March 2021

Revised Date: 10 August 2021

Accepted Date: 13 August 2021

Please cite this article as: { doi: https://doi.org/

Journal of the European Ceramic Society, Volume 41, Issue 15, December 2021, pp. 7412-7422
DOI:10.1016/j.jeurceramsoc.2021.08.018

Fabrication and characterisation of high-performance joints made of ZrB_2-SiC ultra-high temperature ceramics

Xiaochao Jin[1], Jingjing Yang[1,*], Yongle Sun[2,*], Pan Li[1], Cheng Hou[1], Yuxiang Zhao[1], Xueling Fan[1]

[1] State Key Laboratory for Strength and Vibration of Mechanical Structures, School of Aerospace Engineering, Xi'an Jiaotong University, Xi'an 710049, China

[2] Welding Engineering and Laser Processing Centre, School of Aerospace, Transport and Manufacturing, Cranfield University, Cranfield, MK43 0AL, UK

* Corresponding authors.

E-mail address: jing_jing_y@mail.xjtu.edu.cn (J.J. Yang); yongle.sun@cranfield.ac.uk (Y.L. Sun).

Abstract: Joining is crucial for ultra-high temperature ceramics (UHTCs) to be used in demanding environments due to the difficulty in manufacturing large and complex ceramic components. In this study, ZrB_2-SiC composite UHTCs parts were joined via Ni foil as filler, and the mechanical properties and oxidation behaviour of the fabricated ZrB_2-SiC/Ni/ZrB_2-SiC (ZS/Ni/ZS) joint were investigated. Firstly, dense ZrB_2-SiC composites were prepared from nano-sized powders by spark plasma sintering (SPS). The ZrB_2-SiC parts were then joined using SPS. Furthermore, the elastic modulus, hardness, shear strength and high temperature oxidation behaviour of the ZS/Ni/ZS joint were examined to evaluate its properties and performance. The experimental results showed that the ZrB_2-SiC parts were effectively joined via Ni foil using SPS and the resultant microstructures were free from any marked defects or residual metallic layers in the joint. Although the elastic modulus and hardness in the joining zone were lower than those in the base ZrB_2-SiC ceramics, the shear strength of the joint reached ~161 MPa, demonstrating satisfactory mechanical properties. Oxidation tests revealed that the ZS/Ni/ZS joint possesses good oxidation resistance for a wide range of elevated temperatures (800 − 1600 °C), paving the way for its employment in extreme environments.

Keywords: Ultra-high temperature ceramics, high-performance joint, spark plasma joining, mechanical properties, high temperature oxidation.

1 Introduction

Ultra-high temperature ceramics (UHTCs), including borides, carbides, and nitrides of early transition metals [1-3], have a high melting point over 3000 °C. Due to their excellent thermal, mechanical and chemical stability, UHTCs have been considered as the most promising candidate materials for applications facing ultra-high temperature environments, such as the thermal protection for hypersonic aerospace vehicles, and the core components in propulsions and advanced nuclear fuels [4-9]. So far, many methods have been developed to fabricate UHTCs, among which the spark plasma sintering (SPS) is the most advantageous method, since it can realize full densification, reduce sintering temperature and time, and improve mechanical and thermal stability [10-12]. As one type of UHTCs, diborides, such as ZrB_2, have been proven to be highly resistant to oxidation [13-15]. During the sintering process of ZrB_2, SiC is often introduced as a second phase, since it inhibits grain growth, improves sinterability, and enhances the oxidation and mechanical properties [16-18]. Therefore, ZrB_2-SiC composites have attracted the widest attention for research and applications of UHTCs. However, it is still challenging to fabricate UHTCs with complex shape or large size, hence limiting the envisioned potential of UHTCs.

Joining UHTCs or UHTCs/alloys enables UHTCs to be assembled into a complex shape or assembled with a large size. In recent years, remarkable progress has been made in joining of engineering ceramics, especially for UHTCs [19-21]. Active metal brazing and diffusion bonding are widely used for joining of ceramics [22-23]. Among all the high temperature brazing filler metals (Ti, Ni, Cu, Zr, Nb, Ag, Hf, Pd, etc.), Ni is recognized as an ideal interlayer in diffusion bonding of alloys and ceramics to obtain high quality joints for high temperature applications [29–30], due to its high melting temperature, low vapor pressure and good ductility [24-28]. It has been reported that Ni can effectively wet ZrB_2 and HfB_2 ceramics [31-34]. As a result, Ni has been used as braze to join ZrB_2-based UHTCs [35-37]. These previous studies have demonstrated that UHTCs can be joined using brazing filler metals and achieve a good set of mechanical properties. However, one drawback of such type of joining method is that a residual metal interlayer remains trapped in the joint, which may cause the degradation of the high temperature performance of the joined structure [25], owing to the metal interlayer softening or oxidation. Such a drawback can be overcome via pressure-assisted sintering methods for most UHTCs [35], which can distribute the residual metallic interlayer by increasing the joining time or temperature. Among them, SPS is a promising fabrication method,

since it can be implemented at lower temperatures and requires shorter joining time, as compared with hot pressing [38].

The mechanical and chemical properties of UHTCs joints are crucial to their performance and service life, which are also of critical importance to the constructed thermal protection systems. Shear strength is a key index to evaluate the mechanical properties of joined structures. Equally importantly, the resistance to high temperature oxidation is a key chemical property index for both the UHTCs and the joined UHTCs components. The local compositions of the ceramic joints, specifically for a Zr-Si-Ni-B-C system, are complicated, leading to complicated oxidation mechanisms. Unfortunately, to the best of the authors' knowledge, no study on the oxidation behaviors of UHTCs joints under different thermal conditions has been ever reported.

In this study, ZrB_2-SiC UHTCs were sintered by SPS and then joined by SPS with a Ni foil as a filler layer. The mechanisms of joining between two ZrB_2-SiC parts via Ni braze were studied. Furthermore, mechanical properties of the ZrB_2-SiC/Ni/ZrB_2-SiC (ZS/Ni/ZS) joint were measured using nano indentation and shear tests. The oxidation behavior of both the base ZrB_2-SiC ceramics and the ZS/Ni/ZS joint for different temperatures and durations of oxidation were also investigated in detail.

2 Experimental procedure

2.1 Materials and sintering

In the SPS process, nano-sized 80 vol.% ZrB_2 powders (0.5 μm, purity > 99%, Forsman Scientific (Beijing) Co. Ltd., China) and 20 vol.% SiC powders (0.5 μm, purity > 99%, Forsman Scientific (Beijing) Co. Ltd., China) were used as the starting materials. In the preparation process, the powders were mixed firstly, and then were ball-milled in absolute ethanol for 12 h using ZrO_2 balls, at a vibration frequency of 30 Hz. Next, the milled powders were dried in a resistance furnace at 120 ℃ for 10 h. Subsequently, the resulting powders were put in a cylindrical graphite die and pre-pressed at room temperature with a pressure of 10 MPa. After that, the pre-shaped cylinder was sintered in a SPS apparatus (LABOX-325S, Sinter Land Inc., Japan). The sintering process includes the following three steps [39]. First, the sample was heated to an intermediate temperature of 1000 °C with a heating rate of 200 °C/min and then was kept for 1 min. Second, the sample was heated to a

peak temperature of 1800 °C in the next 8 min and kept for 15 min. Third, the sample was cooled down to room temperature with a cooling rate of 75 °C/min, as shown in Fig. 1(a). It should be noted that a constant pressure of 40 MPa was applied on the pressure head during the whole sintering stage. The dimensions of the fabricated samples were approximately Φ20 mm × 5 mm.

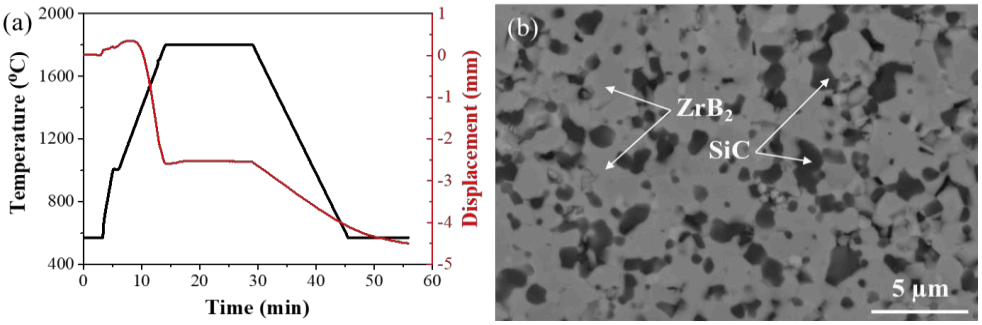

Fig. 1 (a) Temperature and pressure head displacement during sintering process, and (b) microstructure observed of the ZrB_2-SiC ceramics using BSE microscope.

2.2 Joining process

The cylindrical ZrB_2-SiC samples to be joined were polished by diamond grinding discs up to 1500-grit, followed by an ultrasonic cleaning in acetone for 10 min. A Ni foil (30 μm in thickness, purity > 99%, Fuxiang Metal Materials Co., Ltd., China) with dimensions of Φ20 mm × 30 μm was also prepared and cleaned. Two ZrB_2-SiC samples and one Ni foil were assembled in the graphite holder and joined by SPS, forming a ZS/Ni/ZS joint, as shown in Fig. 2(a). The joining process involves a thermal cycle and a pressure load, with temperature and pressure head displacement shown in Fig. 2(b). Firstly, the samples were heated to 1200 °C with a heating rate of 25 °C/min. Then they were kept at the peak temperature for 60 min. Finally, the joint sample was cooled to room temperature with a cooling rate of 75 °C/min. During the joining process, a constant pressure of 10 MPa was applied on the pressure head to enhance the joining effectiveness.

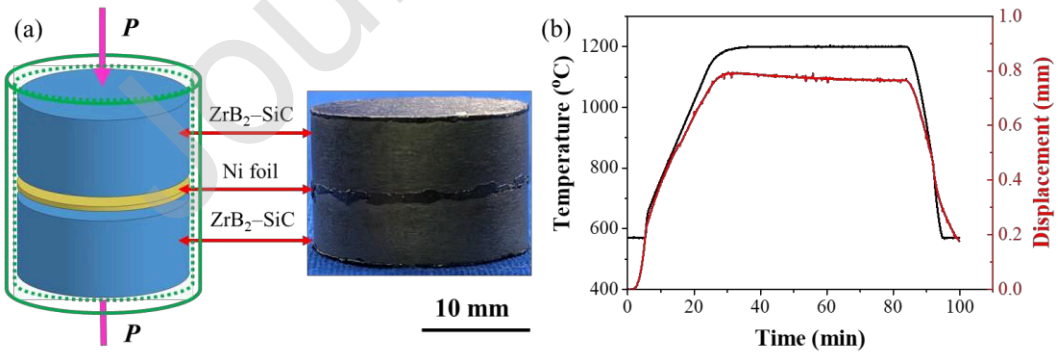

Fig. 2 (a) Joining configurations and (b) temperature and pressure head displacement during the joining process.

2.3 Mechanical properties testing

The elastic modulus and hardness of the base ZrB_2-SiC ceramics and the ZS/Ni/ZS joint were determined by nano indentation tests (Nano Indenter, XP), and then the shear strength of the joint was determined by shear tests (Criterion 45.105, MTS, USA). In order to test the shear strength of the joints, a pair of special nickel-based superalloy loading device is designed, which consists of two fixtures and a baseline substrate, as shown in Fig. 3. In order to meet different shear test requirements, through thickness holes with different sizes were slotted on the two fixtures. In the test, grid paper was used to accurately locate the specimen in the fixtures.

Before the indentation test, the samples were polished by diamond grinding discs up to 2500-grit, followed by an ultrasonic cleaning in acetone for 10 min. The indentation instrument was calibrated before the tests, using a triangular pyramid Berkovich diamond indenter and a standard fused silica sample, with a maximum load of 500 mN. Twenty indentations, with 20 um spacing, on both sides of the joint centreline were tested with a strain rate of 0.05 s^{-1}.

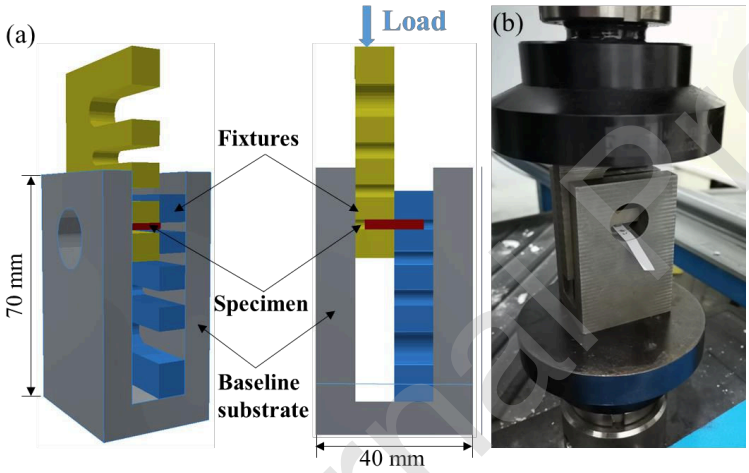

Fig. 3 (a) Schematic of loading device and configurations, and (b) experimental setup of shear test.

The continuous stiffness method (CSM) was adopted such that the elastic modulus and hardness can be continuously measured during the indentation loading [12]. The hardness is defined by

$$H = \frac{P_{\max}}{A_c} \quad (1)$$

where P_{max} is the maximum contact load, A_c is the projected contact area when the load reaches the maximum, viz.

$$A_c = 24.56h_c^2 \quad (2)$$

where h_c is the contact depth which is calculated via

$$h_c = h - \varepsilon \frac{P_{\max}}{S} \quad (3)$$

where h is the maximum indentation depth; ε is a constant for the Berkovich tip; S is the contact stiffness. The reduced modulus can be calculated via

$$E_r = \frac{\sqrt{\pi}}{2\beta} \frac{S}{\sqrt{A_c}} \quad (4)$$

where β is the shape constant of a Berkovich tip. The elastic modulus E of the sample can be calculated using the following relationship

$$\frac{1}{E_r} = \frac{1-\nu^2}{E} + \frac{1-\nu_i^2}{E_i} \quad (5)$$

where E and ν are the elastic modulus and Poisson's ratio of the tested material, respectively; E_i and ν_i are the elastic modulus and Poisson's ratio of the indenter tip, respectively.

The ZS/Ni/ZS joint samples were cut into bricks with dimensions of 11.20 mm × 3.25 mm × 2.75 mm, and then polished by diamond grinding discs up to 1000-grit. Then, the shear strength was tested using a pair of customized holders. In the shear tests, four samples were tested at room temperature at a displacement rate of 0.05 mm/min. The shear strength was obtained via

$$\sigma_s = \frac{F_{\max}}{A_0} \quad (6)$$

where F_{max} and A_0 are the maximum load and cross-sectional area of the ZS/Ni/ZS joint, respectively.

2.4 Oxidation experiments and microscopic characterisation

The ZS/Ni/ZS joint sample was also cut into small bricks with dimensions of 10.0 mm × 2.5 mm × 2.5 mm and polished. The oxidation experiments were performed in an electric furnace (GF 17Q, BOYUNTONG CO., China). The temperature in the furnace increased from room temperature to 1800 °C (± 1 °C) and then was held steady. For each test, the ZS/Ni/ZS joint sample was placed on a

platinum crucible in the furnace. Two groups of experiments were conducted to investigate the effects of oxidation temperature and time on the oxidation behaviour of the ZS/Ni/ZS joint. For the first group (samples #1 – #5), oxidation experiments were conducted at 800 °C, 1000 °C, 1200 °C, 1400 °C and 1600 °C for one hour. For the second group, two samples (#6 and #7) were oxidised at 1600 °C for 0.5 and 2 hours, respectively. The microstructures on the sample surface and the cross-section perpendicular to the joint centre plane were characterised using a scanning electron microscope (SEM, GeminiSEM 500), and the chemical element distributions in the ZS/Ni/ZS joint samples were probed using energy dispersive spectrometer (EDS). The oxidation products were also examined using X-ray diffraction (XRD, D8 ADVANCE, Bruker AXS Inc., Germany) using Cu-Kα radiation (10-90°, 0.02°/step). ImageJ software (National Institutes of Health, USA) was employed to calculate the ceramic grain size on at least 100 grains.

3 Results and discussion

3.1 Joint microstructures and joining mechanisms

Fig. 1(a) shows that the pressure head displacement was almost constant after 20 min at the peak temperature (i.e. 1800 °C), indicating that the ZrB_2-SiC composite densified to a maximum extent. Fig. 1(b) shows the microstructure of the sintered ZrB_2-SiC composite, as observed using back scattered electron (BSE) microscope.

The ZrB_2 and SiC grains in the ZrB_2-SiC composite were uniformly distributed without any obvious defects, as shown in Fig. 1(b). The average bulk density of the ZrB_2-SiC composite was 5.47 g/cm^3, i.e. 98.2% of the theoretical density (5.57 g/cm^3) of ZrB_2-vol. 20% SiC composite. Fig. 4 shows the cross-sectional morphology of a typical ZS/Ni/ZS joint. No macroscopic defects were found on the cross-section, except a small number of micro-sized pores, as shown in Fig. 4(c). The observed microstructure reveals a good quality of joining between the two ZrB_2-SiC parts via the Ni foil. The micro-structural integrity of the joint confirmed the good chemical and mechanical compatibility between ZrB_2-SiC and Ni.

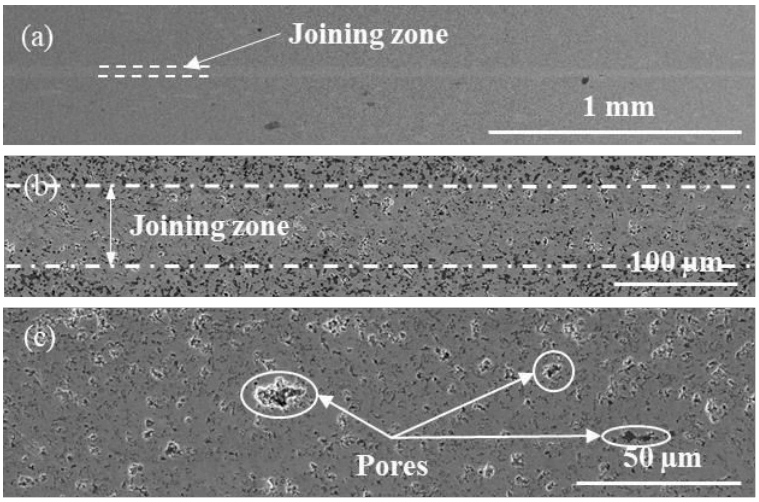

Fig. 4 Cross-sectional morphology of a typical ZS/Ni/ZS joint: (a) and (b) show the joining zone with different magnifications, and (c) shows small pores formed in the joining zone.

Fig. 5 shows the detailed microstructure of the ZS/Ni/ZS joint, as well as the chemical element distributions, on the cross-section. The joining zone and base ZrB_2-SiC ceramics were clearly distinguishable. The thickness of the joining zone falls in the range between 65 μm and 97 μm, with an average of 79 μm. Neither significant residual Ni interlayer nor metal/ceramic interface was observed in Fig. 5(a), thanks to the homogeneous diffusion of Ni element into the ZrB_2-SiC ceramics during the joining process at 1200 °C for 60 min under 10 MPa applied pressure. The diffusion mechanism of Ni element in ZrB_2-SiC ceramics is similar to that of Ni element in the Ni–SiC [35], B-Ni-Zr [33], B-Ni-Ti, B-Ni-Zr and Ni-B-Hf systems [34]. The SiC grains in the joining zone were almost depleted and some graphite particles formed, in contrast to the base ZrB_2-SiC ceramics, as confirmed by the EDS determined chemical element distributions, as shown in Fig. 5. Detailed profiles of the chemical element distributions in the base ZrB_2-SiC ceramics and joining zone are shown in Figs. 6 and 7, respectively. The distributions of Si and Zr elements further confirmed that the base ZrB_2-SiC ceramics was composed of ZrB_2 and SiC particles with an approximately uniform distribution (Fig. 6). The distribution of ZrB_2 appears independent of the joining process, i.e., the distribution of Zr element was consistent between the base ZrB_2-SiC ceramics and the joining zone (Fig. 6 and Fig. 7, respectively). For the joining zone, it is interesting to see that the Si and Ni elements exhibited similar distributions, and some graphite particles were also formed. It is surmised that Ni reacted with SiC and new reaction product could be formed during the joining process. Based on the thermodynamic calculations on the standard Gibbs free energy change (ΔG) for the chemical

reactions, the most possible reactions at 1200 °C are as follows,

$$SiC + Ni = NiSi + C; \quad \Delta G = -31.5 \text{ kJ mol}^{-1} \quad (7)$$

$$SiC + 2Ni = Ni_2Si + C; \quad \Delta G = -69.5 \text{ kJ mol}^{-1} \quad (8)$$

$$NiSi + Ni = Ni_2Si; \quad \Delta G = -42.9 \text{ kJ mol}^{-1} \quad (9)$$

According to the most negative change of standard Gibbs free energy, Ni_2Si is the most thermodynamically stable product among all the possible Ni-containing silicides [25]. According to the EDS analysis results, the molar ratio of Ni to Si is about 2:1, which confirms the formation of graphite and Ni_2Si phases. The XRD pattern on the cross section also showed that Ni_2Si phase (PDF number: 65-1507) formed in the joining zone. These results are consistent with the previous experimental results on joining of ZrC-SiC ceramics with Ni foil filler using hot pressing and electroplating assisted diffusion bonding [24,25]. In the joining process developed here, the grain size of ZrB_2 in the base ZrB_2-SiC ceramics remained basically unchanged, 1.18 μm (after sintering) to 1.20 μm (after joining), while the grain size in the joining zone obviously decreased, with an average value of 0.85 μm. Comparing the microstructures shown in Figs. 6 and 7, one can see that more micro-sized pores formed in the joining zone, due to the diffusion of Ni into the adjacent base material. Compared with the NiSi ($T_{melting}$ = 980 °C), Ni_2Si ($T_{melting}$ = 1300 °C) has much higher melting point; therefore, the Ni_2Si might restrain excessive diffusion of Ni at high temperature, which is beneficial to the ZS/Ni/ZS joint [35].

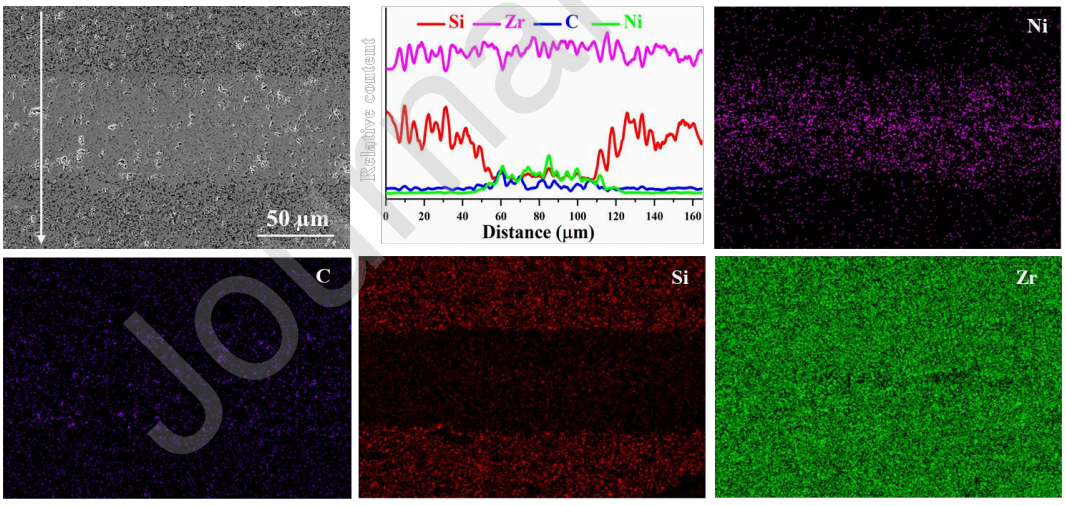

Fig. 5 Microstructure and chemical element distributions of joining zone.

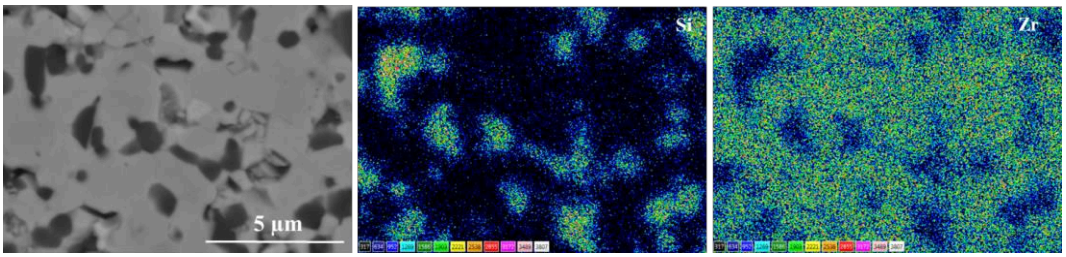

Fig. 6 Microstructure and chemical element distributions in the base ZrB_2-SiC ceramics.

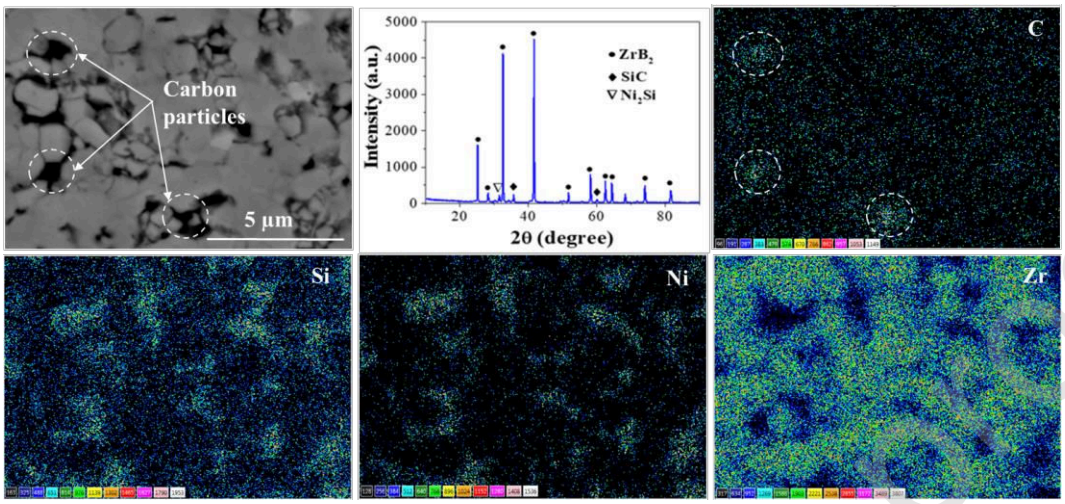

Fig. 7 Microstructure, XRD spectrum and chemical element distributions in a region within the joining zone.

Compared with the hot pressing and other joining methods for UHTCs [33,35], the SPS process led to favourable joint microstructures, due to several effects. First, the electric field of SPS could enhance the diffusivity of Ni elements to the base ceramics by electro migration phenomena, thus promoting migration of ions through the joining interface [40,41]; second, the homogeneous microstructure of the joint was also due to the use of a metallic foil instead of a powder[33,35,36]. The prevention of significant residual Ni layer in the joint made by the SPS process implies two benefits at least: (1) no residual metallic interlayer means that the residual stress gradient would be lower, which is generally beneficial to mechanical properties, since the thermal expansion coefficients of ZrB_2 (5.9×10^{-6} /°C) and SiC (4.3×10^{-6} /°C) [3] are much lower than that of Ni (13.3×10^{-6} /°C) [42]; (2) the Ni-induced softening phenomenon, due to melting of Ni below 1000 °C, could be retarded and thereby the service temperature of the ZS/Ni/ZS joint could be increased.

3.2 Mechanical properties

Fig. 8(a) shows the load-displacement curves obtained in the nano indentation tests, as performed at different locations in the joining zone and base ZrB_2-SiC ceramics. It is evident that the slopes of

the load-displacement curves for the joining zone are less steep than those for the base ceramics, meaning that the elastic modulus and hardness are lower for the former than for the latter. The measured elastic modulus and hardness at the locations with different distances from the joint centreline are shown in Fig. 8(b). It is clearly seen that, overall, both elastic modulus and hardness increase with the increase in distance from the joint centreline. In the joining zone, the elastic modulus varied from 313 to 398 GPa, with an average of 342±26 GPa, while the hardness varied from 10 to 17 GPa, with an average of 12±2 GPa. In the base ceramics, the average elastic modulus was 473±33 GPa, while the average hardness was about 19±2 GPa. This is partly caused by the porosity and the formation of Ni-silicides, since the hardness and elastic modulus of Ni-based silicides are much lower: the hardness and elastic modulus are only 2 GPa and 210 GPa for Ni substrate[43], while the elastic modulus of Ni_2Si is about 61 GPa [44]. The morphologies of the indents in the joining zone and the base ceramics were also compared, as shown in Figs. 8(c) and (d), respectively, and the area of the indent in joining zone was larger than that in base ZrB_2-SiC ceramics.

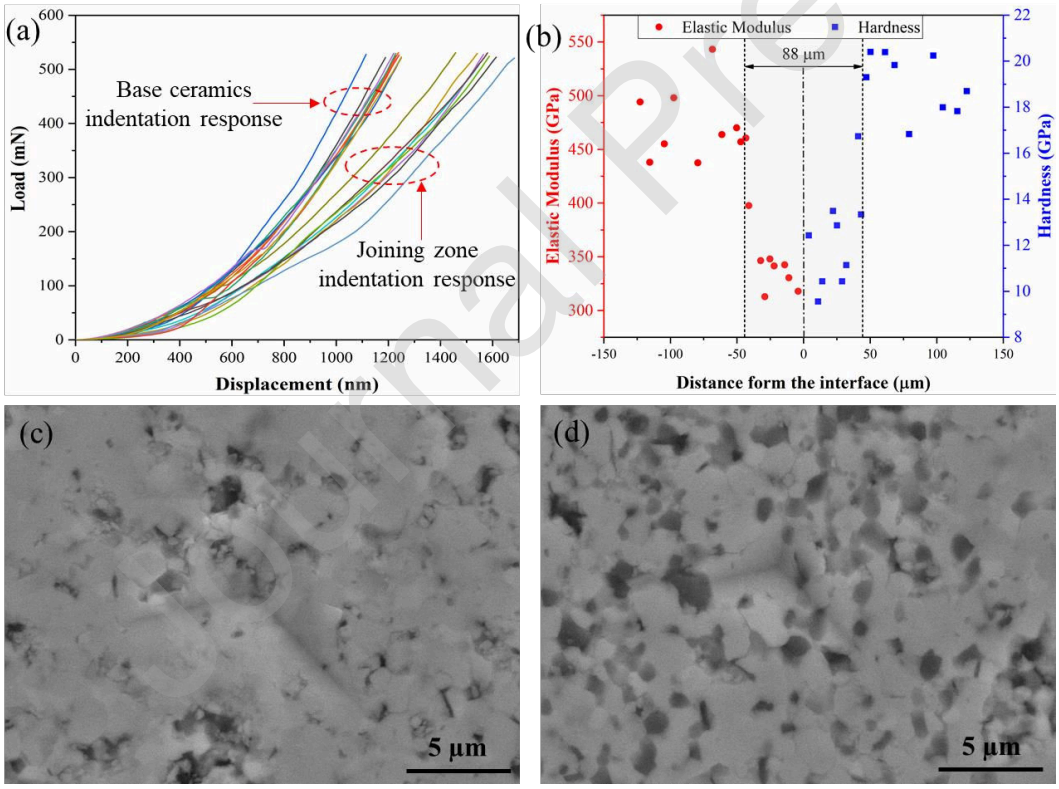

Fig. 8 Nano indentation tests: (a) load-displacement curves, (b) elastic modulus and hardness in terms of the distance from the joint centreline, (c) and (d) show indents in ZS/Ni/ZS joining zone and base ZrB_2-SiC ceramics, respectively.

The shear test revealed that the ZS/Ni/ZS joint suffered from brittle fracture, similar to the failure mode of ZrB_2-SiC ceramics. The average of the measured shear strength was 161.1±9.6 MPa for the fabricated ZS/Ni/ZS joint samples, which is much higher than the reported shear strength (i.e. around 60 MPa) of the ZS/Ni/ZS joints fabricated by hot pressing with Ni powder [35] and close to the shear strength (158 MPa) of TiB whiskers reinforced ZS/Nb/ZS joints [45].

The fracture surface of the joint was overall rough; however, due to the deflection of the crack, the local fracture surface on one side of the sample was deflected toward the base ZrB_2-SiC ceramics, and the fracture surface in this region was relatively smooth (Fig. 9(a)). Looking at the fracture surface of ZS/Ni/ZS joints, the cracks were deflected locally and bypassed the fine grains during the fracture process; in other words, the joining zone mainly exhibited intergranular fracture, as shown in Fig. 9(b). During the fracture process, the crack actively bypassed the ZrB_2 particles with smaller grain size, but it propagated across ZrB_2 particles grains grain size, as shown in Fig. 9(c).

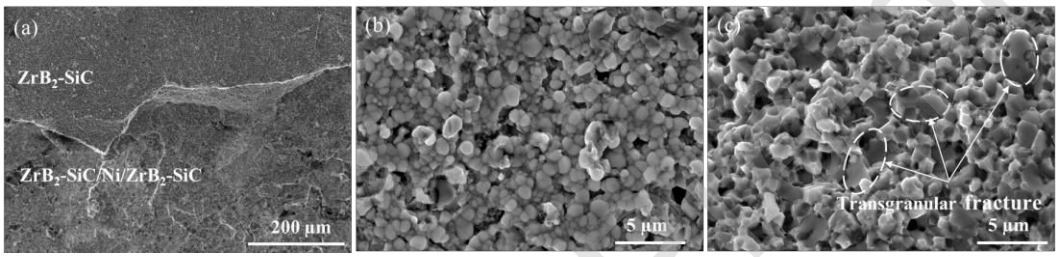

Fig. 9 (a) macro morphology of shear failure surface, (b) micro morphology in ZS/Ni/ZS joining zone and (c) micro morphology in base ZrB_2-SiC ceramics. Circled grains evidence a transgranular fracture opposed to a generally intergtranular one observed for fine ZrB_2 grains.

3.3 Oxidation behaviour

The photos of the ZS/Ni/ZS joint samples before and after oxidation for different temperatures and durations are shown in Fig. 10. The brightness and roughness of the sample surface increased with the increase of oxidation temperature and time. No cracks or other macro defects formed after the oxidation, which demonstrated a good oxidation resistance of the ZS/Ni/ZS joint. The oxide layer thickness measured from the cross-sectional SEM images and mass gain per unit area of the oxidised ZS/Ni/ZS joint samples increased with the increase in oxidation temperature and time, as shown in Fig. 11. The fastest oxidation occurred when the temperature exceeded 1200 ^{o}C, as shown in Fig. 11(a). For an oxidation temperature of 1600 ^{o}C, the mass gain per unit area was approximately proportional to the oxidation time; while the thickness of oxide layer increased with oxidation time in a nonlinear manner, as shown in Fig. 11(b). It should be noted that the scatter in oxide layer

thickness increased with both oxidation temperature (Fig. 11a) and time (Fig. 11b).

More detailed characterisation and analyses of the oxidation behaviour are presented as follows.

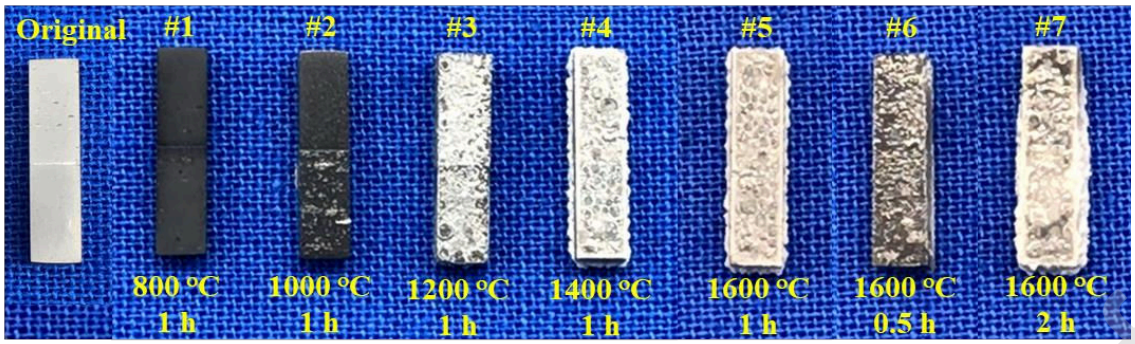

Fig. 10 Photos of ZS/Ni/ZS joint samples before and after oxidation at different temperatures.

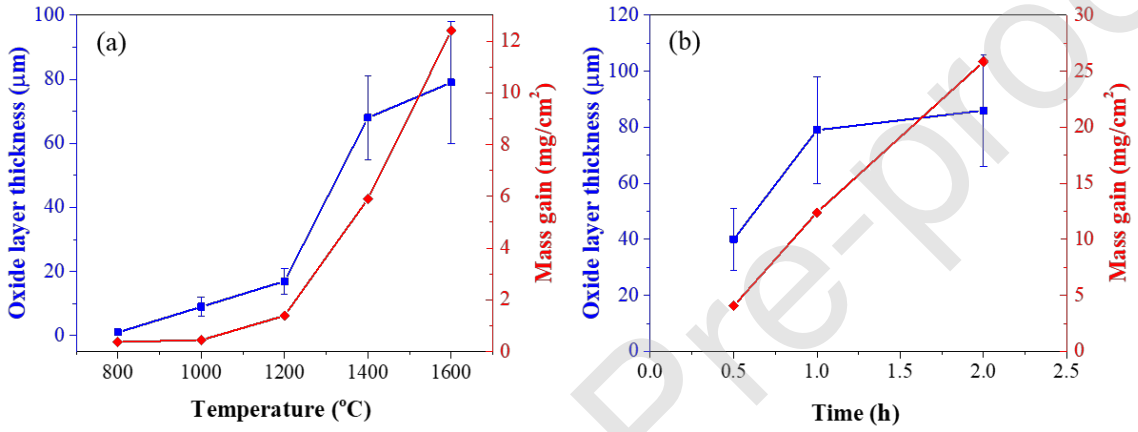

Fig. 11 The oxide layer thickness and mass gain per unit area of ZS/Ni/ZS joint samples after oxidation: (a) at different temperatures for 1 hour and (b) at 1600 °C for different durations.

(1) Oxidation at 800 °C

Generally, the oxidation of ZrB_2-SiC ceramics is negligible below 800 °C, as confirmed by thermogravimetric analysis (TGA) of SiC powder, ZrB_2 powder, and ZrB_2-SiC ceramics [46-48]. When the temperature is between 800 °C and 1200 °C, ZrB_2 oxidises faster than SiC [48-50]. At an oxidation temperature of 800 °C, the base ZrB_2-SiC ceramics oxidized slowly with no obvious changes in the macrostructure, as shown in Fig. 12(a), and the typical reaction for the ZrB_2 oxidation is given below

$$ZrB_2 + 5/2\ O_2 = ZrO_2 + B_2O_3 \quad (10)$$

This reaction has been confirmed by a low mass gain per unit area (0.45 mg/cm^2) after 1-hour oxidation at 800 °C. Microscopic observation further confirmed that amorphous solid B_2O_3 (melting temperature ~450 °C) formed on the sample surface, as shown in Fig. 12(b). However, the main

micro-constituents were ZrB_2, SiC, Ni and Ni-containing compounds; being the amount of B_2O_3 not sufficient to form a continuous oxide layer, due to its high vaporization rate of B_2O_3. After oxidation, no discernible changes of microstructures or chemical elements distributions were observed in the joining zone, as shown in Fig. 12 (c).

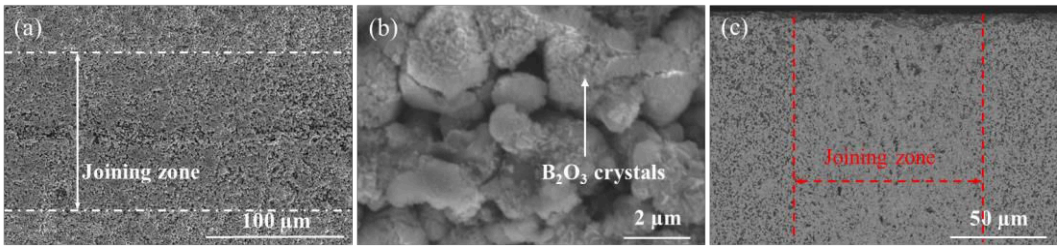

Fig. 12 Microstructures after oxidation at 800 °C for 1 h: (a) exposed surface of ZS/Ni/ZS joint, (b) magnification of the local surface in joining zone, and (c) cross-sectional morphology of the joining zone.

Previous studies [51,52] have shown that Ni oxidizes to form NiO with a low reaction rate, as shown in Reaction (11) at 800 °C.

$$Ni + 1/2\ O_2 = 2\ NiO \quad (11)$$

Due to the formation of continuous SiO_2 and B_2O_3 films, any Ni-compound in the bulk can be protected. Consequently, the oxidation of Ni could be neglected when the temperature was below 1000 °C. As listed in Reactions (7)-(9), Ni_2Si and NiSi existed in the joining zone, and some carbon particles formed due to the reaction between Ni and SiC during the joining. Therefore, diverse reactions occurred during the high temperature oxidation of the ZS/Ni/ZS joint samples, as shown in Reactions (12)-(14). All the associated changes in Gibbs free energy are negative at 800 °C, meaning that these oxidation reactions are thermodynamically possible in the considered environment.

$$C + O_2 = CO_2 \quad (12)$$

$$Ni_2Si + 2\ O_2 = SiO_2 + 2\ NiO \quad (13)$$

$$NiSi + 3/2\ O_2 = SiO_2 + NiO \quad (14)$$

(2) Oxidation at 1000 °C

At 1000 °C, the oxidation of ZrB_2 is faster than that at 800 °C. As a result, a thin B_2O_3 layer mixed with ZrO_2 can form [48,49]. Fig. 13(a) shows that some small ZrO_2 particles preferentially formed near the joint centreline, due to the low content of SiC in the joining zone. The cross-sectional microstructures of the base ZrB_2-SiC ceramics and joining zone are illustrated in Figs. 13(b) and (c), respectively. It can be observed that a ZrO_2 layer with a small amount of B_2O_3 formed

on the surface of the parent ceramic. EDS analysis also showed that no Ni element could be detected on the oxidized sample surface in the joint. As shown in Fig. 13(c), the joining zone containing Ni became wider due to the diffusion in the oxidation process.

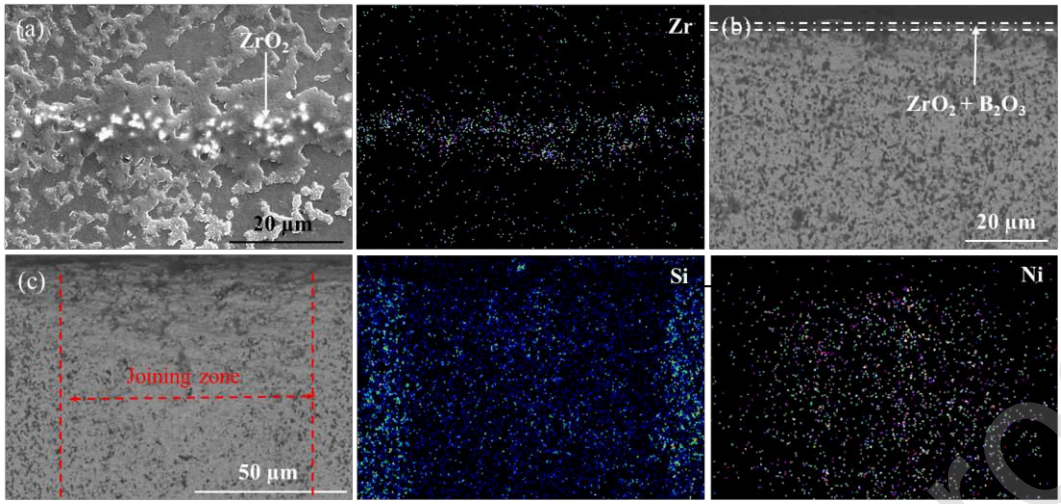

Fig. 13 Microstructures after oxidation at 1000 oC for 1 h: (a) exposed surface of ZS/Ni/ZS joint and corresponding Ni element distribution, (b) cross-sectional polished morphology of base ZrB_2-SiC ceramics, (c) cross-sectional morphology of joining zone, and distributions of Si and Ni elements.

(3) Oxidation at 1200 °C

At a temperature of 1200 °C and beyond, SiC started to oxidise quickly [48-50], according to the Reaction (15). At this temperature, the oxidation of SiC became faster than ZrB_2, as confirmed by the fluctuation of the TGA weight gain curve of ZrB_2-SiC ceramics [46,48].

$$SiC + 2O_2 = SiO_2 + CO_2 \quad (15)$$

Fig. 14(a) shows that some small Ni containing bubbles were detected in the joining zone on the sample surface. Cross-sectional morphology of base ZrB_2-SiC ceramics and joining zone after oxidation are shown in Figs. 14(b) and (c). It is evident that a thin SiO_2 layer formed on the surface. Below the SiO_2 layer, a mixed SiO_2 and ZrO_2 scale was found, in agreement with previous studies on the oxidation of similar systems [48-50]. Due to the high vapour pressure and high volatility, no B_2O_3 could be observed in the oxide layer [50]. For the joining zone, only a single layer of SiO_2–ZrO_2 can be observed in the cross-section after oxidation, in which Ni was almost absent. Since the structural integrity of the oxidation layer was damaged during the cutting process, no SEM images were presented here.

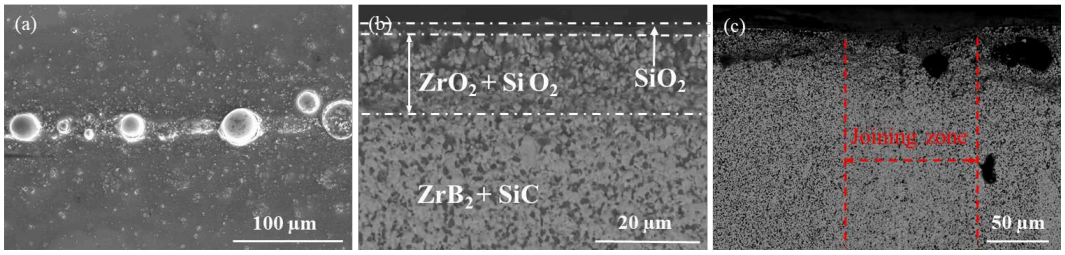

Fig. 14 Microstructures after oxidation at 1200 °C for 1 h: (a) surface of ZS/Ni/ZS joint, (b) and (c) cross-sectional morphologies of the base ZrB_2-SiC ceramics and joining zone.

(4) Oxidation at 1400 °C

At 1400 °C, the oxidation becomes more aggressive. The rapid oxidation was confirmed by the marked increase of the oxide layer thickness and mass gain per unit area of ZS/Ni/ZS joint, as shown in Fig. 11(a). According to common literature and confirmed by the chemical element distribution maps shown in Fig. 15(a), the oxide layer of base ZrB_2-SiC ceramics can be divided into three sub-layers: SiO_2, SiO_2–ZrO_2 and ZrO_2 sub-layers. It is interesting to see that a thin SiO_2-depleted layer containing only ZrO_2 was found at 1400 °C. As illustrated in Fig. 15(b), a solid glassy SiO_2 sub-layer was also formed on the sample surface within the joining zone. The thickness of the SiO_2 sub-layer was not uniform. In addition, Ni elements were detected in the supposed SiO_2–ZrO_2 sub-layer for the joining zone. According to the aforementioned analysis, the Ni-containing component is expected to be NiO formed from the oxidation of any Ni-compound.

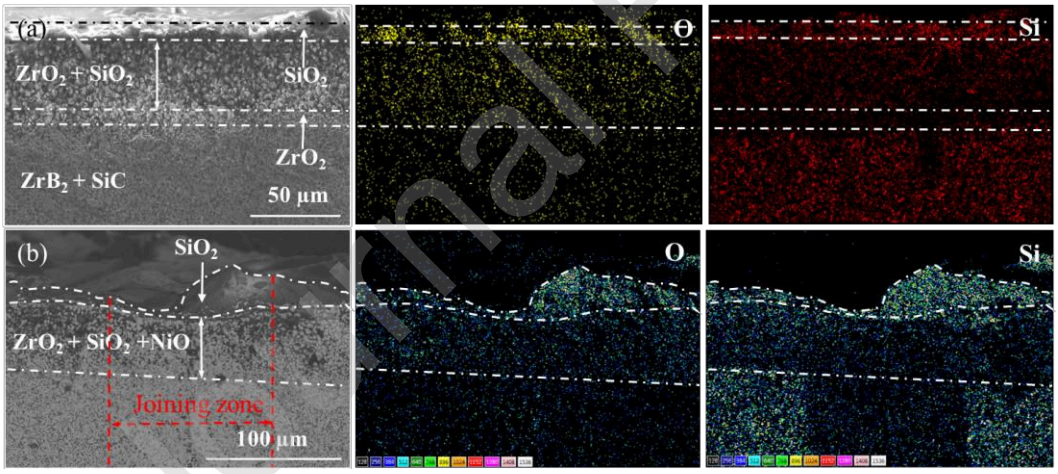

Fig. 15 Cross-sectional morphologies and distribution maps of chemical elements after oxidation at 1400 °C for 1 h: (a) base ZrB_2-SiC ceramics and (b) joining zone.

(5) Oxidation at 1600 °C

After oxidation for 0.5, 1 and 2 hours at 1600 °C, the oxide layer of base ZrB_2-SiC ceramics maintained the above mentioned 3-layered architecture, as shown in Figs. 16(a) – (c). However, the innermost ZrO_2 sub-layer, comprising only ZrO_2, is quite different from the commonly observed

SiC-depleted sub-layer, in which only ZrB_2 exists[48-50]. SiC-depleted (ZrB_2) sub-layer forms only when the partial pressure of O_2 is in the range of 4.1×10^{-14} – 1.8×10^{-11} Pa and the temperature is higher than 1500 °C, according to the volatility diagram for SiC [49]. When the partial pressure of O_2 is within this range, SiC can be oxidized by Reaction (16).

$$SiC\ (s) + O_2\ (g) = SiO\ (g) + CO\ (g) \quad (16)$$

SiO is then transported from the SiC surface to the upper SiO_2 sub-layer, due to the chemical potential gradients of O_2 and SiO across the depleted region; as a result, the SiC-depleted sub-layer forms[48,49]. On the contrary, in the present samples tested here, only ZrO_2 could be detected in the third sub-layer, which indicated that both ZrB_2 and SiC oxidised; with the major oxidation product of SiC being gaseous SiO, rather than SiO_2.

In the joining zone, the outermost glassy SiO_2 layer was still present after oxidation for 0.5 h at 1600 °C, as shown in Fig. 16(d), but it disappeared after oxidation for 1 h, as shown in Figs. 16(e) and (f). Such a microstructural difference can be attributed to the low SiC content in the joining zone. The oxidation of the joint became more aggressive after the protective glassy SiO_2 layer disappeared. Therefore, it could be inferred that the service life of the ZS/Ni/ZS joint at 1600 °C is limited, although no obvious defects could be observed in the joint after 2 h oxidation.

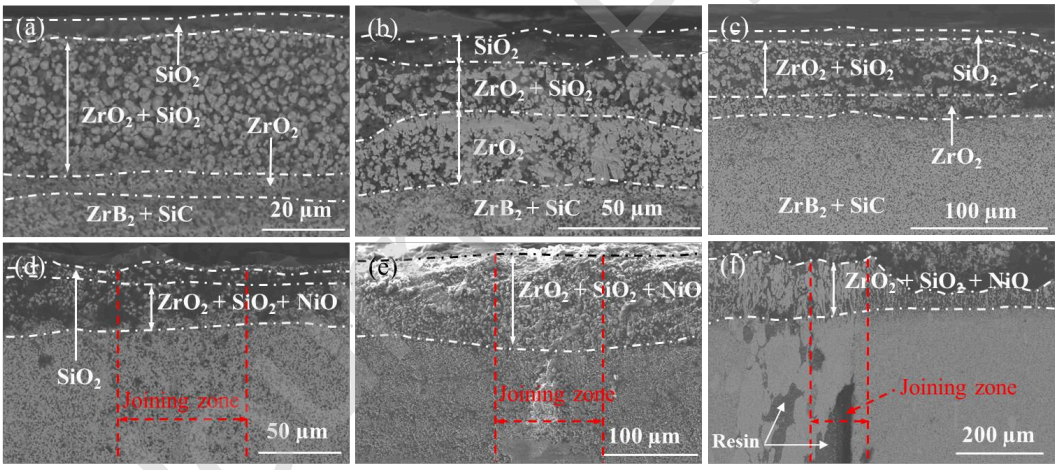

Fig. 16 Cross-sectional morphologies after oxidation at 1600 °C: (a)-(c) base ZrB_2-SiC ceramics oxidised for 0.5, 1 and 2 h, respectively; (d)-(f) joining zone oxidised for 0.5, 1 and 2 h, respectively.

In the oxidation processes at different temperatures, Ni element continued to diffuse into the base ZrB_2-SiC ceramics and reacted with SiC grains, and the Ni-compounds near the surface oxidised resulting in the formation of a ZrO_2-SiO_2-NiO oxide layer. The oxidation of the ZrB_2 and SiC dominated the oxidation process in the joining zone, as the content of Ni and Ni-compounds was

relatively low in the ZS/Ni/ZS joint. In the joining zone, SiC grains had reacted with Ni in the joining process, leading to the different oxidation behaviours (i.e. different architectures of oxide layer) between ZS/Ni/ZS joint and ZrB_2-SiC ceramics. Especially, when the temperature is above 1600 ^oC, the SiO_2 layer could not be maintained when the oxidation time exceeded 1 h, since the SiC content in the joint was relative low. Overall, the experimental results showed that the oxidation resistance of the ZS/Ni/ZS joint was good since no defects formed after oxidation under different thermal conditions, thanks to the good integration of the initial metallic Ni into the ceramics and formation of Ni-silicides.

The oxidation tests demonstrated that the ZS/Ni/ZS joint prepared by the SPS could be used in high temperature applications due to the high oxidation resistance of the joint, consisting of only ceramic phases, ZrB_2 SiC and Ni_xSi_y However, more caution should be taken when temperature is higher than 1600 ^oC, which is actually the use limit for SiC, since no top SiO_2 layer could serve for oxidation protection purpose.

4 Conclusions

Ultra-high temperature ceramics based on ZrB_2-SiC, were prepared by SPS at 1800 °C, and then the prepared ZrB_2-SiC parts were joined by SPS at 1200°C for 1 h dwell using a 30 μm thick Ni foil as filler, thereby forming a high performance ZS/Ni/ZS joint. The main conclusions are drawn as follows:

(1) ZrB_2-SiC sintered parts were effectively joined by SPS with Ni foil filler, and the proposed simple fabrication method avoided macro defects and did not leave residual metallic layers in the joint, due to the formation of Ni_2Si as major reaction product between the original Ni and SiC grains. The elastic modulus and hardness in the joining zone were lower than those in the base ZrB_2-SiC ceramics, while the shear strength of the joint reached about 161 MPa, outperforming other pressure-assisted sintering methods or those using powder as filler.

(2) The oxidation mechanisms of the ZS/Ni/ZS joint were different from those of ZrB_2-SiC ceramics due to the reaction between Ni and SiC grains in the joining process, resulting in the formation of different scale architectures. The oxidation of the ZrB_2 and SiC dominated the oxidation process of the ZS/Ni/ZS joint, since SiO_2 and ZrO_2 determined the scale architectures of the oxide layers.

(3) The ZS/Ni/ZS joint possesses good oxidation resistance at temperatures up to 1600 °C for 0.5 h. Above 1600 °C, the joint area was strongly damaged due to the absence of a protective outermost scale.

Declaration of Interest Statement

The authors declare that there is no conflict of interest regarding the publication of this article.

Acknowledgments

This work is supported by supported by National Science and Technology Major Project (J2019-IV-0003-0070), the National Natural Science Foundation of China (Grant Nos. 1171101165 and 11602188), the China Postdoctoral Science Foundation (2021M692571). The authors would like to thank Prof. James Marrow, Dr. Boxuan Li and Abdalrhaman Mohamed in the University of Oxford, for their help in nano indentation tests.

References

[1] W.G. Fahrenholtz, E.J. Wuchina, W.E. Lee, Y. Zhou, Ultra-High Temperature Ceramics: Materials for Extreme Environments. John Wiley & Sons, Inc., Hoboken, NJ, 2014.

[2] W.G. Fahrenholtz, G.E. Hilmas, Ultra-high temperature ceramics: Materials for extreme environments. Scr. Mater. 129 (2017) 94–99.

[3] X.C. Jin, X.L. Fan, C.S. Lu, T.J. Wang, Advances in oxidation and ablation resistance of high and ultra-high temperature ceramics modified or coated carbon/carbon composites. J. Eur. Ceram. Soc. 38 (2018) 1-28.

[4] J.F. Justin, A. Jankowiak, Ultra high temperature ceramics: densification, properties and thermal stability. Aerosp. Lab J. 3 (2011) 1-8.

[5] S.R. Levinea, E.J. Opila, M.C. Halbig, J.D. Kiser, M. Singh, J.A. Salem. Evaluation of ultra-high temperature ceramics for aeropropulsion use. J. Eur. Ceram. Soc. 22 (2002) 2757–2767.

[6] S.F. Tang, C.L. Hu. Design, Preparation and Properties of Carbon Fiber Reinforced Ultra-High Temperature Ceramic Composites for Aerospace Applications: A Review. J. Mate. Sci. Technol. 33 (2017) 117–130.

[7] I.M. Low, Y. Sakka, C.F. Hu, MAX Phases and Ultra-High Temperature Ceramics for Extreme Environments. IGI Global, Hershey, 2013.

[8] T.H. Squire, J. Marschall. Material property requirements for analysis and design of UHTC components in hypersonic applications. J. Eur. Ceram. Soc. 30 (2010) 2239–2251

[9] A. Paul, D.D. Jayaseelan, S. Venugopal, E. Zapata-Solvas, J. Binner, B. Vaidhyanathan, A. Heaton, P. Brown, W.E. Lee, UHTC composites for hypersonic applications. Am. Ceram. Soc. Bull. 91 (2012) 22-29.

[10] M.J. Gasch, D.T. Ellerby, S.M. Johnson, Ultra high temperature ceramic composites, in: N.P. Bansal (Ed.), Handbook of Ceramic Composites. Springer, Boston, MA, 2005, pp. 197–224.

[11] L. Zhang, N.P. Padture, Inhomogeneous oxidation of ZrB_2-SiC ultra-high-temperature ceramic particulate

composites and its mitigation. Acta Mater. 129 (2017) 138-148.

[12] X.C. Jin, P. Li, C. Hou, X.B. Wang, X.L. Fan, C.S. Lu, G.S. Xiao, X.F. Shu, Oxidation behaviors of ZrB_2 based ultra-high temperature ceramics under compressive stress. Ceram. Int. 45 (2019) 7278–7285.

[13] G.J. Zhang, D.W. Ni, J. Zou, H.T. Liu, W.W. Wu, J.X. Liu, T.S. Suzuki, Y. Sakka, Inherent anisotropy in transition metal diborides and microstructure/property tailoring in ultra-high temperature ceramics - a review. J. Eur. Ceram. Soc. 38 (2018) 371-389.

[14] R. Chaim, G. Chevallier, A. Weibel, C. Estournes. Grain growth during spark plasma and flash sintering of ceramic nanoparticles: a review. J. Mater. Sci. 53 (2018) 3087–3105.

[15] J.K. Sonber, A.K. Suri. Synthesis and consolidation of zirconium diboride: review. Adv. Appl. Ceram. 110 (2011) 321-334.

[16] S.Q. Guo. Densification of ZrB_2-based composites and their mechanical and physical properties: A review. J. Eur. Ceram. Soc. 29 (2009) 995–1011

[17] K.X. Gui, F.Y. Liu, G. Wang, Z.J. Huang, P. Hu. Microstructural evolution and performance of carbon fiber-toughened ZrB_2 ceramics with SiC or $ZrSi_2$ additive. J. Adv. Ceram. 7 (2018) 343–351.

[18] X.J. Yan, X.C. Jin, P.Li, C.Hou, X. Hao, Z.G. Li, X.L. Fan. Microstructures and mechanical properties of ZrB2-SiC-Ni ceramic composites prepared by spark plasma sintering. Ceram. Int. 45 (2019) 16707–16712.

[19] J.A. Fernie, R.A.L. Drew, K.M. Knowles. Joining of engineering ceramics. Int. Mater. Rev. 54 (2009) 283-331.

[20] A. Passerone, F. Valenza, M.L. Muolo. A review of transition metals diborides: from wettability studies to joining. J. Mater. Sci. 47 (2012) 8275–8289.

[21] D. Sciti, L. Silvestroni, L. Esposito, K. Nakashima, N. Saito, Y. Yamaoka, A.M. Glaeser. Advances in transient-liquid-phase bonding of ultra-high temperature ZrC ceramics. High Temp. Mater. Proc. 31 (2012) 501–511.

[22] O.M. Akselsen. Diffusion bonding of ceramics. J. Mater. Sci. 27 (1992) 569–579.

[23] W.B. Hanson, K.I. Ironside, J.A. Fernie. Active metal brazing of zirconia. Acta Mater. 48 (2000) 4673–4676.

[24] C.B. Song, T.S. Lin, P. He, W.Q. Yang, D.C. Jia, J.C. Feng. Microstructure evolution and its effect on the mechanical properties of the ZrC–SiC composite joint diffusion bonded with pure Ni foil. Ceram. Int. 40 (2014) 17–23.

[25] C.B. Song, P. He, T.S. Lin, H.M. Wei, W.Q. Yang. Electroplating assisted diffusion bonding of ZrC–SiC composite for full ceramic joints. Ceram. Int. 40 (2014) 7613–7616.

[26] C.B. Song, P. He, T.S. Lin, D.C. Jia. Interfacial reaction evolution of the ZrC ceramic joint diffusion bonded with Ni interlayer. Ceram. Int. 40 (2014) 12999–13007.

[27] R. Asthana, M. Singh. Joining of ZrB_2 based ultra-high-temperature ceramic composites using Pd-based braze alloys. Scr. Mater. 61 (2009) 257-260.

[28] L. Silvestroni, D. Sciti, L. Esposito, A.M. Glaeser, Joining of ultra-refractory carbides. J. Eur. Ceram. Soc. 32 (2012) 4469-4479.

[29] M.I. Osendi, A.D. Pablos, P. Miranzo, Microstructure and mechanical strength of Si_3N_4/Ni solid state bonded interfaces. Mater. Sci. Eng. A 308 (2001) 53–59.

[30] Z. Zhong, T. Hinoki, H. Jung, Y. Park, A. Kohyama. Microstructure and mechanical properties of diffusion bonded SiC/steel joint using W/Ni interlayer. Mate r. Des. 31 (2010) 1070–1076.

[31] A. Passerone, M.L. Muolo, F. Valenza, F. Monteverde, N. Sobczak. Wetting and interfacial phenomena in Ni–HfB_2 systems. Acta Mater. 57 (2009) 356-364.

[32] N. Saito, H. Ikeda, Y. Yamaoka, A.M. Glaeser, K. Nakashima. Wettability and transient liquid phase bonding of hafnium diboride composite with Ni–Nb alloys. J. Mater. Sci. 47 (2012) 8454–8463.

[33] F. Valenza, M.L. Muolo, A. Passerone, G. Cacciamani, C. Artini. Control of interfacial reactivity between ZrB_2 and Ni-based brazing alloys. J. Mater. Eng. Perform. 21 (2012) 660-666.

[34] A. Passerone, M.L. Muolo, F. Valenza. Critical issues for producing UHTC-brazed joints: wetting and reactivity. J. Mater. Eng. Perform. 25 (2016) 3330–3347.

[35] B. Yuan, G.J. Zhang, Microstructure and shear strength of self-joined ZrB_2 and ZrB_2-SiC with pure Ni. Scr. Mater. 64 (2011) 17-20.

[36] P. Li, X. Jin, C. Hou, H. Li, X. Yan, M. Yuan, X. Fan, Cyclic thermal shock behaviors of ZrB_2-SiC ultra-high temperature ceramics joints bonded with Ni interlayer. J. Alloy. Compd. 793 (2019) 49-55.

[37] W.Q Yang, T.S Lin, P. He, H.M. Wei, L.L. Xing, D.C. Jia. Microstructure and mechanical properties of ZrB_2–SiC joints fabricated by a contact-reactive brazing technique with Ti and Ni interlayers. Ceram. Int. 40 (2014) 7253–7260.

[38] W.R. Pinc, M.D. Prima, L.S. Walker, Z.N. Wing, E.L. Corral. Spark plasma joining of ZrB_2–SiC composites using zirconium–boron reactive filler layers. J. Am. Ceram. Soc. 94 (2011) 3825–3832.

[39] X.C. Jin, Y.L. Sun, C. Hou, X.B. Wang, G.Y. He, X.L. Fan. An investigation into the cooling-rate dependent residual stresses in ZrB_2–SiC composites using an improved Raman spectroscopy method. Ceram. Int. 45 (2019) 22564–22570.

[40] Z.A. Munir, U. Anselmi-Tamburini. The effect of electric field and pressure on the synthesis and consolidation of materials: A review of the spark plasma sintering method. Journal of Mater. Sci. 41 (2006) 763-777.

[41] S. Rizzo, S. Grasso, M. Salvo, V. Casalegno, M.J. Reece, Mo. Ferraris. Joining of C/SiC composites by spark plasma sintering technique. J. Eur. Ceram. Soc. 34 (2014) 903-913.

[42] P. Hidnert. Thermal expansion of some nickel alloys. J. Res. Natl. Inst. Stand. Technol. 58 (1957) 2737.

[43] Y.Y. Zhang, F.M. Heim, J.L. Bartlett, N.N. Song, D. Isheim, X.D. Li. Bioinspired, graphene-enabled Ni composites with high strength and toughness. Sci. Adv. 2019; 5: eaav5577.

[44] S.Z. Han, J. Kang, S.D. Kim, S.Y. Choi, H. G. Kim, J. Lee, K. Kim, S.H. Lim, B. Han. Reliable and cost effective design of intermetallic Ni2Si nanowires and direct characterization of its mechanical properties. Sci. Rep. 5 (2015) 15050.

[45] P. He, W. Yang, T. Lin, D. Jia, J. Feng, Y. Liu. Diffusion bonding of ZrB_2–SiC/Nb with in situ synthesized TiB whiskers array. J. Eur. Ceram. Soc. 32 (2012) 1117-4454.

[46] X.H. Zhang, P. Hu, J.C. Han. Structure evolution of ZrB_2–SiC during the oxidation in air. J. Mater. Res. 23, (2008) 1961-1972.

[47] C.L. Hu, S.F. Tang, S.Y. Pang, H.M. Cheng. Long-term oxidation behaviors of C/SiC composites with a SiC/UHTC/SiC three-layer coating in a wide temperature range. Corros. Sci. 147 (2019) 1-8.

[48] A. Rezaie, W.G. Fahrenholtz, G.E. Hilmas. Evolution of structure during the oxidation of zirconium diboride–silicon carbide in air up to 1500 ◦C. J. Eur. Ceram. Soc. 27 (2007) 2495–2501.

[49] W.G. Fahrenholtz. Thermodynamic analysis of ZrB_2–SiC oxidation: formation of a SiC-depleted region. J. Am. Ceram. Soc., 90 (2007) 143–148.

[50] D.E. Glass. Physical challenges and limitations confronting the use of UHTCs on hypersonic vehicles. 17th AIAA international space planes and hypersonic systems and technologies conference. San Francisco, CA, 2011.

[51] S. Chevalier, F. Desserrey, J. P. Larpin. Oxygen transport during the high temperature oxidation of pure nickel. Oxid. Met. 64 (2005) 219-234.

[52] D. Serafin, W. J. Nowak, B. Wierzba. The effect of surface preparation on high temperature oxidation of Ni, Cu and Ni-Cu alloy. Appl. Surf. Sci. 476 (2019) 442–451.

2021-08-16

Fabrication and characterisation of high-performance joints made of ZrB2-SiC ultra-high temperature ceramics

Jin, Xiaochao

Elsevier

Jin X, Yang J, Sun Y, et al., (2021) Fabrication and characterisation of high-performance joints made of ZrB2-SiC ultra-high temperature ceramics. Journal of the European Ceramic Society, Volume 41, Issue 15, December 2021, pp. 7412-7422

https://doi.org/10.1016/j.jeurceramsoc.2021.08.018